ELSEVIER

Applied Surface Science 175–176 (2001) 663–669

applied surface science

www.elsevier.nl/locate/apsusc

Unoccupied states evolution with oxidation of ultrathin Mg, Zn and Cd layers on $SrTiO_3(100)$ surfaces

P.J. Møller[a,*], S.A. Komolov[b], E.F. Lazneva[b], A.S. Komolov[b]

[a]*Department of Chemistry, University of Copenhagen, Universitetsparken 5, DK-2100 Copenhagen, Denmark*
[b]*Research Institute of Physics, St. Petersburg University, Uljanovskaja street 1, St. Petersburg 198904, Russia*

Accepted 20 November 2000

Abstract

An unoccupied density of states (DOS) evolution under oxidation of ultrathin Mg, Zn and Cd layers on $SrTiO_3(1\,0\,0)$-(2×2) substrates are investigated. The metal deposition and subsequent oxidation were studied in situ under UHV conditions by means of LEED, AES, TCS and work function measurements. An appearance of metal- and oxygen-derived bands of the unoccupied DOS was traced in the TC spectra. Metal oxidation was followed by the hybridization of metal and oxygen orbitals and by the appearance of the mainly O 2p oxygen-derived bands, which are characterized by a set of DOS maxima, located at the following energies (above the Fermi level): 8.0, 11.5, 14.3, 15.0 and 19.0 eV for MgO; 6.0, 8.1, 16.8 and 20.5 eV for ZnO and 7.5, 10.0 and 12.7 eV for CdO. The results obtained are discussed in comparison with previously published experimental and theoretical data on unoccupied DOS in metal oxides.

Keywords: Density of unoccupied states; Metal oxide surfaces; Total current spectroscopy

1. Introduction

The energy structure of unoccupied electronic states is of particular interest as far as these states are very sensitive to the local bonding environment, such as the number of valence electrons, their spin configuration, and the symmetry and coordination number of the structural unit cell. Experimental studies of unoccupied states are usually performed by using near-edge X-ray absorption fine structure (NEXAFS), inner-shell electron energy-loss spectroscopy (ISEELS), appearance potential spectroscopy (APS), inverse photoemission spectroscopy (IPES), bremsstrahlung isochromat spectroscopy (BIS) [1,2] and total current spectroscopy (TCS) [3–5]. The excitation process in NEXAFS, ISEELS and APS involves electronic transitions from a core state to an unoccupied state above the Fermi level, and they are governed by the dipole selection rule. In addition, an unoccupied density of states (DOS) may be affected by core-hole effects. In IPES and BIS, electron transitions occur from higher to lower states which both are located above the Fermi level, and the final DOS determination requires a knowledge of the higher (initial) states from which de-excitation of the electrons occur. These problems may be avoided by using a low-energy electron reflection technique which does not involve preliminary electronic excitation in the solid surface under study and in which only one electronic state is involved (electron transition from vacuum into the solid). An accurate study of the energy dependence of

* Corresponding author. Fax: +45-35320299.
E-mail address: pjm@kiku.dk (P.J. Møller).

0169-4332/01/$ – see front matter
PII: S0169-4332(01)00123-4

the electron reflection may be performed by a TCS technique in which the energy dependence of current transmitted through a sample is analyzed over the 0–30 eV range [3–6].

The electronic energy structure of metal oxides is characterized by an alternation of pronounced bands and gaps of unoccupied DOS, being located above the Fermi level and been created due to the process of hybridization of metal and oxygen orbitals. Our results on studies of unoccupied states in CuO, MgO films and in single crystals of ZnO and α-Fe_2O_3 have been published recently [7–9]. In the present communication we analyze an unoccupied DOS evolution under oxidation of ultrathin Mg, Zn and Cd layers on $SrTiO_3$(1 0 0) substrates. An emphasis is placed on the clearing up of the oxygen derived contributions into unoccupied DOS in course of thin metal layers oxidation.

2. Experimental

The investigations were carried out in a UHV system (base pressure 10^{-8} Pa) that combines different surface analytical techniques. A four-grid low-energy electron diffraction (LEED) system can be switched between the LEED mode and an operational mode in which TC spectra are measured. Auger electron spectroscopy (AES) characterization of the surface under study was performed using a double-pass cylindrical mirror analyzer. The experimental set-up has previously been described in more detail [10]. In the TCS experiment, a well-collimated beam of slow electrons is directed onto the surface under study, and the total current $J(E)$ in the sample circuit is monitored as a function of incident-electron energy E in the range 0–30 eV [3,4,11,12]. In order to reveal the fine structure present in the total current, the first derivative of the current, $S(E) = \mathrm{d}J/\mathrm{d}E$, is measured using lock-in amplification technique. $S(E)$ is referred to as the TCS signal. In our equipment an electron beam current of 1–10 nA (beam energy was modulated at 800 Hz, 0.1 eV peak-to-peak) was incident normal to the surface, focused into a 0.2–0.4 mm diameter spot. Such gentle probing of the sample by TCS provided a non-destructive surface characterization. The 'primary' peak in TCS indicates the vacuum level E_{vac} of the surface under study. Its shift along the retarding-voltage scale corresponds to the work-function variation due to surface treatment. In order to obtain the absolute values of the work-functions, the Fermi level E_F was calibrated with respect to both the tungsten cathode and to a freshly deposited gold film.

The fine structure of the TC-spectrum is determined by the energy dependence of the electron reflection coefficient. The latter is represented by the sum of two components, one being the elastic reflection and the other the inelastic one. At low primary energies ($E < 20$–25 eV) the elastic reflection component may be considered as predominant [3–5]. An energy dependence of the elastic reflection is closely related to the energy band structure of the solid in the energy range corresponding to the primary electron energy [3–6]. We are dealing with the electronic states of solids located above the vacuum level (unoccupied DOS). If in the energy range under consideration there is an energy gap, then the electrons are totally reflected. When reaching the allowed band, the elastic reflection decreases abruptly and transmission electron current increases. The energy dependence of the transmitted current $J(E)$ will be determined by the density of unoccupied states (DOS). Therefore, the $(S(E) = \mathrm{d}J/\mathrm{d}E)$ maxima will be associated to the energy location of the unoccupied band edges, and the maxima of $(-\mathrm{d}S(E)/\mathrm{d}E)$ will be associated to the energy location of DOS maxima. Thus, the negative derivative of the TCS signal is more suitable for comparison to the theoretically and experimentally derived DOS (using other techniques for unoccupied DOS studies). Further details of TCS experiments and of TC spectra interpretations in relation to the surface electronic structure have been discussed elsewhere [3–7,11,12].

2.1. Substrate

Cleaning of the strontium titanate (MaTeck, Germany) substrate surface was performed in a UHV-chamber using a photo–thermo etching in oxygen, $P(O_2) = 10^{-5}$ Pa, and a subsequent annealing process [13]. The obtained LEED pattern of the $SrTiO_3$(1 0 0) surface was characterized by a (2×2) reconstruction which corresponds to an oxygen deficient $SrTiO_3$(1 0 0) surface. A corresponding AES-spectrum in the energy range of 300–1200 eV is shown

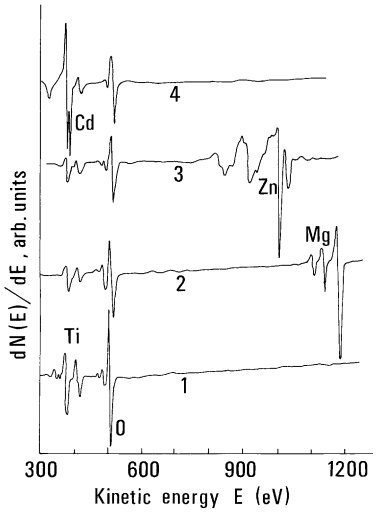

Fig. 1. Auger electron spectra in the energy range 300–1200 eV from: (1) $SrTiO_3$(1 0 0) substrate; (2) deposited layers of Mg; (3) Zn and (4) Cd. The spectra are normalized to the amplitude of more intensive peak.

in Fig. 1 by the curve 1 (strontium Auger lines in the vicinity of 100 eV are not shown, they are similar to the previously reported ones [13]). The data on the intensity ratios of the Auger lines indicated clearly that we are dealing with an oxygen deficient $SrTiO_3$(1 0 0)-(2 × 2) surfaces were easily reproducible and they were used as substrates for deposition of Mg, Zn and Cd metal overlayers.

2.2. Metal layer deposition

Deposition of Mg, Zn and Cd overlayers was performed in situ by thermal sublimation from a specially designed evaporator. In the course of metal deposition the substrate LEED picture was gradually attenuated until it vanished due to the formation of disordered overlayers. In the case of Cd deposition, however, it was not possible to obtain a complete surface coverage, and the LEED picture from the substrate was attenuated but still seen after further deposition of Cd. The observed behavior can be explained by taking into account an extremely small sticking probability of Cd atoms to the $SrTiO_3$ surface. Deposition of Cd was followed by the decrease of the work function (WF) to the value 3.0 ± 0.1 eV which corresponds to about 0.5 monolayer (ML) coverage. Metal coverage was estimated from AES intensity relations, quartz microbalance data and from the attenuation of the TCS signal of the substrate. The WF for the Mg deposit was characterized by a curve with a minimum at ML coverage 2.2 ± 0.1 eV and by saturation value of 2.6 ± 0.1 eV at an average thickness 2.5–3 ML (the WF of clean $SrTiO_3$(1 0 0)-(2 × 2) surface was measured as 4.1 ± 0.1 eV). A small increase of the WF up to 4.2 ± 0.1 eV was observed during Zn layer deposition (the average thickness was about 2.5–3 ML). Deposited metal layers were characterized by Auger spectra which are presented in Fig. 1, curves 2 (Mg), 3 (Zn) and 4 (Cd). All presented spectra contain the deposited metal Auger lines as predominant ones and the substrate lines which are strongly attenuated but are still seen. One can conclude that the deposited metals did not cover continuously the substrate.

2.3. Metal layer oxidation

Oxidation of the metal overlayers was performed by oxygen inlet into the UHV-chamber to the pressure $P(O_2) = 10^{-3}$ Pa and under the following condition: sample temperatures 300, 425 and 500 K for Cd, Zn and Mg, respectively, and O_2 exposure 1 h. After the oxidation procedure, the system was evacuated to the base pressure of about 10^{-7} Pa. After oxidation of the metal layers an appearance of a LEED pattern was observed only in case of the Mg-deposit. There was a MgO(1 0 0)-c(2 × 2) superstructure. ZnO_x and CdO_x layers were characterized by disordered structures. The oxidation was followed by a strong increase of the oxygen Auger line. Taking into account the AES sensitivity factors for elements [14] and AES intensity ratio of oxygen and the metal for the pure oxides under study, it is possible to estimate the compositions of oxidized surfaces to $(MgO)_{86}(TiO_2)_7(SrO)_7$, $(ZnO)_{78}$-$(TiO_2)_{12}(SrO)_{10}$ and $(CdO)_{45}(TiO_2)_{30}(SrO)_{25}$, respectively. A small amount of CdO on the $SrTiO_3$ surface is due to a small Cd-metal saturation coverage which was limited by the weak interaction between Cd and the $SrTiO_3$ substrate. After oxidation, the WF of the samples under study became equal to 3.3 ± 0.1, 3.8 ± 0.1 and 3.6 ± 0.1 eV for MgO, CdO and ZnO, respectively. The obtained values of the WF for the thin-film Mg–MgO and Zn–ZnO systems are in agreement with previously reported data [15–17]. It should be mentioned that a MgO surface layer is more

stable on the $SrTiO_3$ surface without any decomposition or desorption up to a temperature of about 1000 K, while the CdO and ZnO layers are weakly bonded. The CdO layer was completely desorbed from the $SrTiO_3$ surface, a temperature of about 500 K, and the ZnO layer at a temperature of about 600–650 K.

3. Result and discussion

3.1. TC spectra evolution during metal layer deposition and oxidation

TC spectra were monitored through the process of metal (Mg, Zn or Cd) deposition onto the $SrTiO_3(1\,0\,0)$-(2×2) substrate and its subsequent oxidation. A set of TC spectra is presented in Fig. 2. Curve 1 is the spectrum of the substrate. It was shown recently [18] that this spectrum contains maxima which are related to the Ti-derived (a: Ti 3d and a_1: Ti 4s), Sr-derived (b, b_1, b_2: Sr 4d triplet and b_3: Sr 5p) and O-derived (c, c_1: O 2p) empty electronic bands. It should be mentioned that the TC maximum location corresponds to the bottom edge of the band of unoccupied DOS.

During metal deposition the fine structure of the substrate spectrum was gradually attenuated and new maxima being the characteristic for deposited metal appeared. In Fig. 2 (curves 2, 3 and 4) the spectra are shown for the Cd, Zn and Mg layers, respectively. In the Cd-spectrum, the most pronounced maximum, marked by B, can be related to the Cd 5p empty states. When the Cd-coverage is about 0.5 ML, the fine structure of the substrate is not completely attenuated and some of the substrate maxima are still seen in the spectrum (curve 2). On the other hand, a coverage of 2.5–3 ML is enough for complete attenuation of the TC spectrum from the substrate (curves 3 and 4 for Zn and Mg, respectively). In the spectrum from the Zn layer, there are two main maxima A and B which can be related to the Zn 4s and Zn 4p empty bands [7]. The maxima B and D for the Mg layer can be connected with the Mg 3p and Mg 3d empty bands, respectively [7].

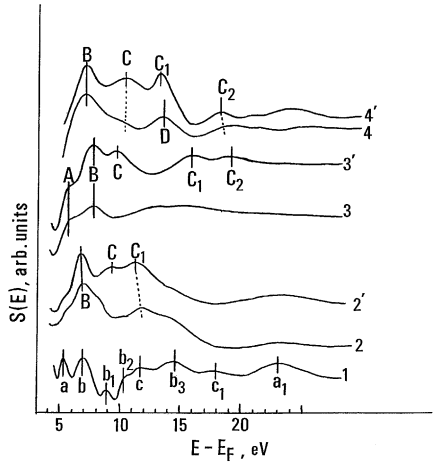

Fig. 2. TC spectra $S(E)$ from: (1) $SrTiO_3(1\,0\,0)$ substrate; (2) metal deposited layers of Cd; (3) Zn and (4) Mg and after their oxidation: CdO (2′), ZnO (3′) and MgO (4′).

Oxidation of the thin metal overlayers was accompanied by the following evolution of the TC spectra: (1) the main metal-derived maxima became more pronounced and narrow, pointing to hybridization of oxygen (O 2p) and metal orbitals [19]; (2) appearance of the set of oxygen-derived maxima C, C_1 and C_2. The spectra from the oxidized layers are presented in Fig. 2 by the curves 2′ (CdO), 3′ (ZnO) and 4′ (MgO). The spectrum obtained from the oxidized Zn-layer is similar to the spectrum previously reported for single crystal ZnO surfaces [7,20]. It should be noted that the TC spectra from freshly deposited Cd and Mg layers contain weak traces of oxygen-derived maxima: C and C_2 for Mg, and C_1 for Cd, which are shown in Fig. 2 by the dotted lines. The observed features can be explained when taking into account a possibility of spontaneous initial oxidation of Mg and Cd during the deposition via oxygen uptake from the $SrTiO_3$ substrate.

3.2. Oxygen-derived unoccupied electronic states of ZnO, MgO and CdO

Maxima location in the TC spectrum corresponds to the boundary between the gap and the unoccupied band at which an electron reflectivity decreases. In order to reveal precisely the DOS maxima location inside the unoccupied bands, we will consider the negative derivative of TCS $(-\mathrm{d}S/\mathrm{d}E)$. The latter characteristic of TC spectra is most convenient for comparison with data on unoccupied DOS obtained theoretically and experimentally (using other techniques for unoccupied DOS studies).

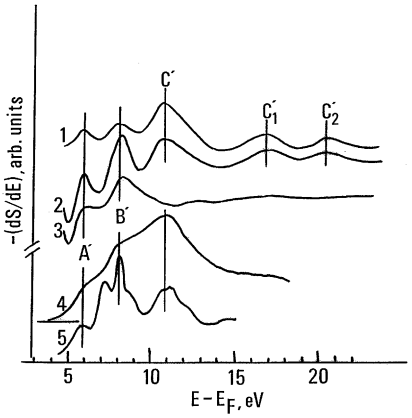

Fig. 3. Curves of $(-\mathrm{d}S/\mathrm{d}E)$ for freshly deposited Zn layer (3), after its oxidation (2) and a difference curve (1) between (2) and (3). NEXAFS data for ZnO [21] (4) and calculated unoccupied DOS [22] (5).

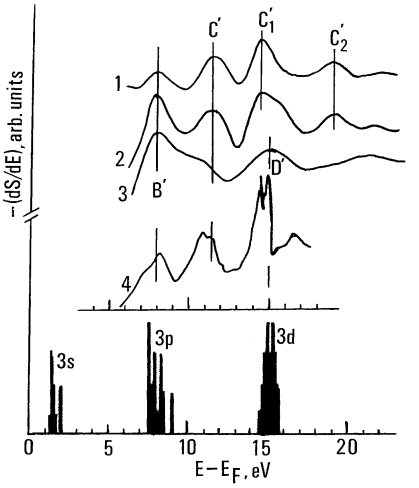

Fig. 4. Curves of $(-\mathrm{d}S/\mathrm{d}E)$ for freshly deposited Mg layer (3), after its oxidation (2) and a difference curve (1) between (2) and (3). Calculated DOS [25] (4) and a histogram of Mg^{2+} excited states [26] (at the bottom of the figure).

3.2.1. ZnO

A set of $-\mathrm{d}S/\mathrm{d}E$ spectra is presented in Fig. 3 for a freshly deposited Zn layer (curve 3), for the layer after oxidation (curve 2) and (curve 1) for the difference between curves 2 and 3. Thus, the difference (curve 1) represents an oxygen contribution into unoccupied DOS due to metal layer oxidation. In Fig. 3, the $(-\mathrm{d}S/\mathrm{d}E)$ curves are considered in comparison with the data on unoccupied DOS in ZnO as derived from NEXAFS measurements (curve 4 [21]) and with the results of a calculation of DOS in ZnO (curve 5 [22]). The main maxima A′, B′ and C′ observed in the $-\mathrm{d}S/\mathrm{d}E$ curves correspond well to the structure of curves 4 and 5. In accordance to the NEXAFS results [21], the observed structure reflects the DOS distribution for empty hybridized orbitals of O 2p and Zn 4sp.

Maxima A′ (6.0 eV) may be related to the Zn 4s–O 2p σ-orbital which corresponds to a σ-type interaction between Zn and O layers. A possible explanation of maximum B′ (8.1 eV) consists of the assumption of a Zn 4p–O 2p π-hybridization. It is an interesting fact that the energy locations of these maxima A′ and B′ was not changed with oxidation and that only their intensities increased. Maximum C′ (11.0 eV) appeared during oxidation and may be directly connected with O 2p-derived states. Two weak maxima C'_1 (16.8 eV) and C'_2 (20.5 eV) appeared also during oxidation and they may be related with antibonding combination of O 2p orbitals in the direct oxygen–oxygen interaction. Appearance of such antibonding bands due to oxygen–oxygen interaction in the energy range 10–20 above the Fermi level was predicted for different metal oxides [23]. A similar doublet structure was reported [26] for the adsorption system O_2/Pt(1 1 1).

3.2.2. MgO

Let us consider the negative derivatives of TCS $(-\mathrm{d}S/\mathrm{d}E)$ for the freshly deposited Mg layer (Fig. 4, curve 3), for the layer after oxidation (curve 2), and the difference curve 1. Mg-derived empty bands of MgO may be presented, in the first approximation, as a result of summation of the excited states of individual Mg^{2+} ions. A histogram of the optical excitation spectra for Mg^{2+} ions is shown in the bottom of Fig. 4, which was used by Henrich et al. [24] for explanation of the Mg 2p electron energy-loss spectrum. One can see that the energy locations of maxima B′ (8.0 eV) and D′ (15.0 eV) in curve 3 correspond well to the position of 3p and 3d empty bands presented in the histogram. An evolution of the $(-\mathrm{d}S/\mathrm{d}E)$ spectrum during oxidation consists of the narrowing of maxima B′ and in appearance of the new maxima C′ (11.5 eV), C'_1 (14.3 eV) and C'_2 (19.0 eV). Maximum C′ is placed between Mg 3p (B′) and Mg 3d (D′) bands, and maximum C'_1 overlaps with the Mg 3d band.

The observed MgO unoccupied DOS is in sufficient agreement with the DOS obtained from a MgO band-calculation [25] which is presented by curve 4 in Fig. 4. Maxima B′ and C′ may be considered as a result of Mg 3p–O 2p hybridization: B′ originates from 3p states at the Mg site with a small mixture of O 2p, and C′ originates from 2p states at the O-site with a small mixture of Mg 3p. It should be noted that the Mg 3d–O 2p band (overlapping maxima C'_1 and D′) is characterized by a relatively weak interaction as they were observed separately. Maximum C'_2 can be connected with an antibonding combination of O 2p orbitals due to oxygen–oxygen interaction. A similar oxygen-derived maximum was observed recently for the adsorption O_2/Mo(1 1 0) system [2]. Another possible explanation of this feature is a hybridization of Mg 4s and O 2p orbitals.

3.2.3. CdO

An evolution with oxidation of an unoccupied DOS of Cd submonolayer is shown in Fig. 5. The $(-dS/dE)$ spectrum for freshly deposited layer (curve 3) contains an attenuated DOS structure of substrate and a main Cd-derived maximum B′ (7.5 eV) reflects, most probably, a Cd 5p unoccupied band. Oxidation of the surface under study was accompanied by an attenuation of the substrate fine structure, by an increase of intensity of maxima B′ (10.0 eV) and C'_1 (12.7 eV) which are clearly seen in the curve 2 and in the difference curve 1. An origin of maxima B′ and C′, likewise to ZnO and MgO, can be explained as hybridized states of Cd 5p and O 2p orbitals. One can see from the Fig. 5 that the maximum C'_1 has the same energy position with the oxygen-derived maximum of the substrate, which becomes more intensive due to oxygen adsorption on the open areas of the $SrTiO_3$ surface.

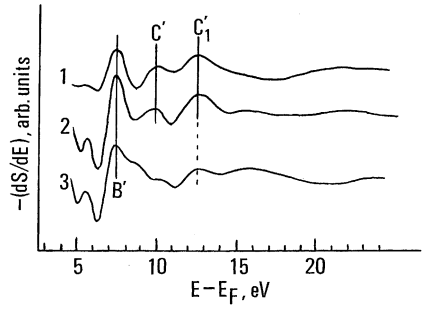

Fig. 5. Curves of $(-dS/dE)$ for freshly deposited Cd layer (3), after its oxidation (2) and a difference curve (1) between (2) and (3).

4. Conclusions

Total current spectroscopy was used to look over an evolution of unoccupied DOS under oxidation of ultrathin Mg, Zn and Cd layers on $SrTiO_3$(1 0 0) substrates. The surfaces under study were monitored by LEED, AES and WF measurements. Oxygen-derived contributions into unoccupied DOS due to metal layers oxidation were determined and they can be divided into two groups. The first one originates via hybridization of O 2p and metal orbits and it consists of unoccupied DOS maxima located at the following energies (above the Fermi level): Zn 4s–O 2p σ (6.0 eV), Zn 4p–O 2p π (8.1 and 11.0 eV), Mg 4p–O 2p π (8.0 and 11.5 eV), Mg 3d–O 2p (14.3 and 15.0 eV) and Cd 5p–O 2p π (7.5 and 10.0 eV). The second one can be connected with an antibonding combination of O 2p orbitals due to oxygen–oxygen interaction and it is presented by the following DOS maxima: 16.8 and 20.5 eV for ZnO, 19.0 eV for MgO and 12.7 eV for CdO surfaces. The results obtained are discussed in comparison with previously published and theoretical data on unoccupied DOS in metal oxides. It was demonstrated that the TCS technique provides more comprehensive and additional information in comparison with NEXAFS, ISEELS and APS techniques as long as TCS does not involve preliminary electronic excitation of the solid and is not limited by the dipole selection rules.

Acknowledgements

The support of the Danish Natural Science Research Council and of the European Commission Brite-Euram programme is gratefully acknowledged.

References

[1] J.C. Fuggle, J.E. Ingelsfield (Eds.), Unoccupied Electronic States: Fundamentals for XANES, EELS, IPS and BIS, Springer, Berlin, 1992.

[2] J.G. Chen, Surf. Sci. Rep. 30 (1997) 1.
[3] S.A. Komolov, Total Current Spectroscopy of Surfaces, Gordon and Breach, Philadelphia, PA, 1992.
[4] S.A. Komolov, V.N. Strocov, Phys. Status Solidi B 167 (1991) 605.
[5] V.N. Strocov, H.J. Starnberg, Phys. Rev. B 52 (1995) 8759.
[6] R.C. Jaklevic, L.C. Davis, Phys. Rev. B 26 (1982) 5391.
[7] P.J. Møller, S.A. Komolov, E.F. Lazneva, J. Phys.: Condens. Matter 11 (1999) 9581.
[8] P.J. Møller, S.A. Komolov, E.F. Lazneva, J. Phys.: Condens. Matter 8 (1996) 6569.
[9] S.A. Komolov, E.F. Lazneva, P.J. Møller, J. Phys.: Condens. Matter 9 (1997) 7297.
[10] P.J. Møller, S.A. Komolov, E.F. Lazneva, E.H. Pedersen, Surf. Sci. 323 (1995) 102.
[11] S.A. Komolov, L.T. Chadderton, Surf. Sci. 90 (1979) 359.
[12] P.J. Møller, M.H. Mohamed, Vacuum 35 (1985) 29.
[13] P.J. Møller, E.F. Lazneva, S.A. Komolov, Surf. Sci. 425 (1999) 15.
[14] C.L. Hedberg (Ed.), Handbook of Auger Electron Spectroscopy, 3rd Edition, Physical Electronics, Eden Prairie, MN, 1995.
[15] R.E. Thomas, J.V. Gibson, G.A. Haas, Appl. Surf. Sci. 5 (1980) 398.
[16] J. Vaari, J. Lathinen, P. Hautojärvi, Surf. Sci. 277 (1992) 253.
[17] D. Briggs, Faraday Discussions 60 (1975) 81.
[18] P.J. Møller, S.A. Komolov, E.F. Lazneva, J. Phys.: Condens. Matter 12 (2000) 7705.
[19] D.W. Fischer, J. Phys. Chem. Solids 32 (1979) 2455.
[20] P.J. Møller, S.A. Komolov, E.F. Lazneva, Surf. Sci. 307–309 (1994) 1177.
[21] J.G. Chen, B. Früberger, M.L. Colaianni, J. Vac. Sci. Technol. A 14 (1996) 1668.
[22] S. Bloom, I. Ortenburger, Phys. Status Solidi B 58 (1973) 561.
[23] F.M.F. de Groot, J. Faber, J.J.M. Michiels, M.T. Czyzyk, M. Abbate, J.C. Fuggle, Phys. Rev. B 48 (1993) 2074.
[24] V.E. Henrich, G. Dresselhans, H.J. Zeiger, Phys. Rev. B 22 (1980) 4764.
[25] S.T. Pantelides, D.J. Miekish, A.B. Kunz, Phys. Rev. B 10 (1974) 5203.
[26] J. Stöhr, NEXAFS Spectroscopy, Springer Series in Surface Science, Vol. 25, Springer, New York, 1992.